# Defective Rock-Salt Structure in Anodically Electrodeposited Mn−Co−O Nanocrystals

## Weifeng Wei,* Weixing Chen, and Douglas G. Ivey

*Department of Chemical and Materials Engineering, University of Alberta, Edmonton, Alberta, Canada T6G 2G6*

*Received: April 6, 2007; In Final Form: May 9, 2007*

Mn−Co−O nanocrystals, ranging from pure cobalt oxides to pure manganese oxides, were anodically electrodeposited on stainless steel substrates. Detailed structural characterization of as-deposited Mn−Co−O nanocrystals was conducted using wavelength-dispersive spectroscopy (WDS), X-ray photoelectron spectroscopy (XPS), and transmission electron microscopy (TEM). WDS and XPS results suggest that there is an inherent cation deficiency associated with the as-deposited nanocrystalline oxides. Experimental selected-area diffraction (SAD) ring patterns obtained from these oxides are consistent with simulated SAD ring patterns of a defective rock-salt-type phase, in which a significant number of cation vacancies reside on the octahedral interstices in the rock-salt-type unit cell. Additional diffracted spots were also observed between the (200) and (220) reflections, which may be attributed to ordering of Mn vacancies in the rock-salt-type unit cell. The formation of this type of defective rock-salt structure is likely a consequence of the low temperatures used to deposit the Mn−Co−O nanocrystals.

## Introduction

Manganese cobalt oxides, $Mn_xCo_{3-x}O_4$ (0 < x < 3), constitute a group of materials that have been widely studied. Spinel-type $Mn_xCo_{3-x}O_4$ (0 < x < 3) has been synthesized by ceramic methods involving solid-state reaction of manganese and cobalt oxide mixtures at 1000 °C.[1−3] In addition, a moderate-temperature method (400 °C) based on thermal decomposition of mixed cobalt−manganese carbonate precursors has been applied to prepare spinel-type manganese cobalt oxides.[4] More recently, the synthesis at low temperature (80−200 °C) of spinel-type cobalt−manganese oxides by coprecipitation with butylamine of mixed cobalt(II)−manganese(II) chloride solutions has also been reported.[5−8] For high-temperature ceramic and moderate-temperature thermal decomposition procedures, a cubic *Fd*3*m* spinel-type solid solution is formed in the compositional range 0 < x < 1.3. A tetragonal *I*4₁/*amd* phase is formed in the interval 1.9 < x < 3.0. For intermediate compositions (1.3 < x < 1.9), mixed cubic and tetragonal spinel-type phases are formed. However, the upper limit for the cubic *Fd*3*m* spinel-like phase synthesized by the low-temperature procedure increases to 1.4, and the lower limit for the tetragonal *I*41/*amd* spinel-type phase increases to 2.0.[5−8] Similar low-temperature procedures, involving the decomposition of cobalt acetylacetonate and manganese acetylacetonate in oleylamine at 200 °C to obtain $CoMn_2O_4$ nanocrystals, have also been reported.[9] It is noted that nanoscale spinel oxides hold many anomalous magnetic properties because of their distinct metastable cation distribution.[9−11] Electrodeposition based on aqueous solutions has also been applied to prepare Mn−Co binary oxide coatings for supercapacitors at room temperature.[12] The high specific capacitance obtained in these oxide coatings was attributed to their amorphous and hydrous natures.[12] Therefore, manganese cobalt oxides are rather sensitive to the synthesis conditions, which can affect the morphology, crystal structure, cation distribution, and oxidation states and, in turn, determine their physicochemical properties.

In one of our previous papers, the synthesis of nanocrystalline coatings in the Mn−Co−O system on ferritic stainless steel substrates by anodic electrodeposition from aqueous solutions has been reported.[13] It was reported that the as-deposited Mn−Co−O nanocrystalline coatings were composed of nanocrystalline oxide grains ranging from a couple of nanometers to 10 nm with a metastable face-centered cubic (fcc) structure. This structure was not sensitive to the deposition parameters. An unambiguous understanding of this metastable fcc phase and phase formation mechanism during anodic electrodeposition is required to study the physicochemical properties of the Mn−Co−O nanocrystals. The aim of this work is to provide some insight into the crystal structure of the metastable phases in the Mn−Co−O system, formed during electrodeposition, ranging from pure cobalt oxides to pure manganese oxides.

## Experimental Procedures

The Mn−Co−O nanocrystals were deposited on ferritic stainless steel substrates, as described previously, using anodic electrodeposition.[13] The solutions consisted of 0.2 M ethylenediaminetetraacetic acid disodium salt and various concentrations of $CoSO_4·7H_2O$ and $MnSO_4·7H_2O$. Seven different Co(II):Mn(II) mole ratios (pure Co(II), 29:1, 9:1, 1:1, 1:9, 1:29, and pure Mn(II)), were used and the total metal ion concentration was set to 0.3 M. The deposition current density, pH value, and temperature of the solutions were adjusted to be 5 mA/cm², 6.0, and 70 °C, respectively. A three-electrode cell configuration, consisting of a platinum counter electrode placed horizontally 20 mm above a horizontal stainless steel working electrode and a saturated calomel electrode (SCE) reference, was used for electrodeposition. Before anodic electrodeposition, the steel substrates were ground with 600-grit SiC abrasive papers, degreased in an alkaline solution at 80 °C, and cleaned ultrasonically in deionized water. The steel substrates were anodically activated in a 0.2 M $H_2SO_4$ solution at a current

* To whom correspondence should be addressed. E-mail: weifeng@ualberta.ca.

Rock-Salt Structure in Mn−Co−O Nanocrystals

*J. Phys. Chem. C, Vol. 111, No. 28, 2007* **10399**

density of 30 mA/cm$^2$ for 2 min and then cathodically activated in a 0.1 M HCl solution at a current density of 30 mA/cm$^2$ for 6 min. The oxide layers were grown to a thickness of 3−4 $\mu$m over a period of 80−90 min. After electrodeposition, the working electrodes were rinsed with deionized water and dried in air.

The morphology was first analyzed in a Hitachi S-2700 scanning electron microscope, equipped with an ultrathin window (UTW) X-ray detector, and a JAMP 9500F field emission scanning Auger microprobe. Quantitative chemical analysis of the as-deposited Mn−Co−O nanocrystals was conducted on a JEOL 8900 microprobe, equipped with five wavelength-dispersive spectrometers. Chemical state analysis was carried out by X-ray photoelectron spectroscopy (XPS) using a Kratos AXIS Ultra X-ray photoelectron spectrometer. A monochromatic Al source, operating at 210 W with a pass energy of 20 eV and a step of 0.1 eV, was utilized. All XPS spectra were corrected using the C 1s line at 284.6 eV. Curve fitting and background subtraction were accomplished by using Casa XPS version 2.3.13 software.

Crystal structure analysis was performed using selected-area diffraction (SAD) patterns. It is well-known that electron-diffracted intensities are highly susceptible to dynamical effects such as multiple scattering.[14] To simplify electron diffraction analysis of Mn−Co−O nanocrystals to a kinematical approximation, SAD patterns were obtained from the thinnest regions. Electron-transparent samples were produced by scraping off the deposits and ultrasonically dispersing them in methanol. One or two drops of the suspension were then deposited on C-coated Cu grids. After evaporation of the methanol, the samples were ready for analysis. Electron diffraction and imaging were performed in a JEOL 2010 transmission electron microscope equipped with a Noran UTW X-ray detector.

## Results and Discussion

**Chemical Analysis.** An example of an as-deposited oxide, prepared from a solution with a Co(II):Mn(II) ratio of 9:1, is shown in Figure 1. Quantitative analysis of Mn, Co, and O elements in the nanocrystalline oxides was done using wavelength-dispersive spectroscopy (WDS). The bulk compositions of the as-deposited nanocrystals are tabulated in Table 1. It is noted that preferential deposition of manganese oxides occurs during anodic electrodeposition even when the Co:Mn ratio in the solution is 9:1. This tendency is consistent with that of the previous study, where the possible preferential deposition mechanism was suggested to be the low dissociation constant ($K_d$) of cobalt sulfate heptahydrate in solution.[13] The oxygen anion to metal cation ratios for all the oxides were calculated to be in the 1.47−1.79 range. This implies that the mean valences of the Mn and Co cations are higher than 2+.

Detailed chemical state analysis of Mn and Co cations in the oxides is shown in Figure 2, where the Co 2p and Mn 3s spectra were taken from typical oxides prepared from pure Co(II), pure Mn(II), and mixed Co(II)−Mn(II) (Co:Mn = 29:1) solutions. The possible variations in oxidation states for Co can be determined from the Co 2p lines in the XPS spectra. For pure cobalt oxides in Figure 1a, the Co 2p spectrum consists of two main spin-orbital lines (M), i.e., 2p$_{3/2}$ and 2p$_{1/2}$, at 780.3 and 795.3 eV, separated by about 15.0 eV, as reported in the literature.[15−17] Two distinguishable satellite peaks were detected at about 5.9 eV (S1) and 9.8 eV (S2) above the Co 2p$_{3/2}$ main peak. The intensity of S1 is much weaker than that of S2. Another satellite peak (S3), with binding energy 9.6 eV higher than that of the Co 2p$_{1/2}$ main peak, was also detected. For the
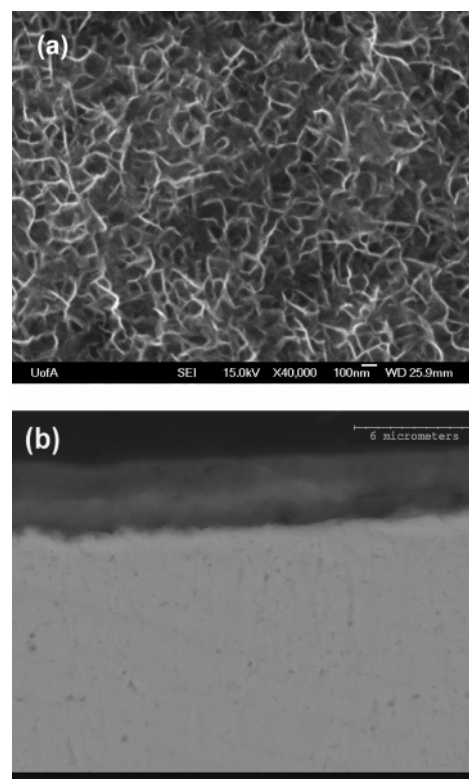


**Figure 1.** Scanning electron microscopy image of an as-deposited oxide prepared from a solution with a Co(II):Mn(II) ratio of 9:1: (a) plan view secondary electron image; (b) cross section back-scattered electron image.

**TABLE 1: Quantitative Analysis of Mn, Co, and O Elements in As-Deposited Oxide Nanocrystals**

| Co(II):Mn(II) ratio (solution composition) | deposit composition (atom %) | | | anion to cation ratio |
|---|---|---|---|---|
| | Mn | Co | O | |
| pure Co(II) | | 40.5 | 59.5 | 1.47 |
| 29:1 | 18.7 | 19.0 | 62.3 | 1.65 |
| 9:1 | 25.3 | 12.9 | 61.8 | 1.65 |
| 1:1 | 35.4 | 4.4 | 60.2 | 1.51 |
| 1:9 | 35.2 | 1.7 | 63.1 | 1.71 |
| 1:29 | 35.5 | 0.3 | 64.2 | 1.79 |
| pure Mn(II) | 36.9 | | 63.1 | 1.71 |

mixed manganese−cobalt oxide (Co:Mn = 29:1), as shown in Figure 2c, the intensity of S1 is higher than that of S2, and the binding energy of S3 is 7.0 eV higher than that of the Co 2p$_{1/2}$ main peak. The binding energy information for the Co 2p spectra taken from these two specimens is summarized in Table 2.

The determination of the oxidation states of Co cations is rather difficult, based merely on the binding energy of the Co 2p peaks, because similar spectra can be obtained from CoO, Co$_3$O$_4$, and Co$_2$O$_3$ oxides. The energy gap between the Co 2p main peak and the satellite peaks is generally considered to be highly related to the oxidation states. When the energy gap is ∼6.0 eV, the Co cation valence is assigned a value of 2+. On the other hand, the spectrum is associated with Co cations having a valence of 3+ if the energy gap is 9−10 eV.[15−27] Therefore, it can be concluded that both Co(II) and Co(III) cations exist in pure cobalt oxide and the mixed manganese−cobalt oxide mentioned above. The only difference is that Co(III) cations are the predominant species in the pure cobalt oxide, while Co-(II) cations are the main cations in mixed manganese−cobalt oxides (Co:Mn = 29:1). This implies that the electrooxidation of Co(II) to a higher oxidation state, i.e., Co(III), was constrained by the presence of Mn(II) ions in the solutions.
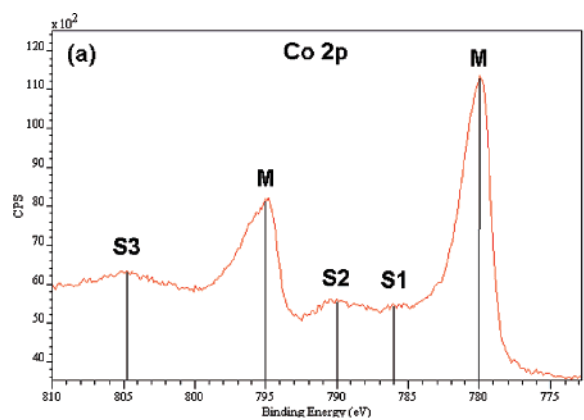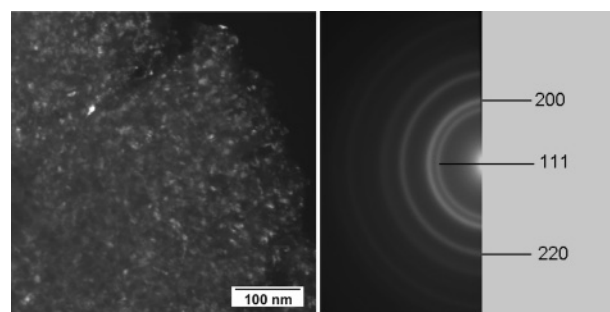
### (a) Pure Co (II)
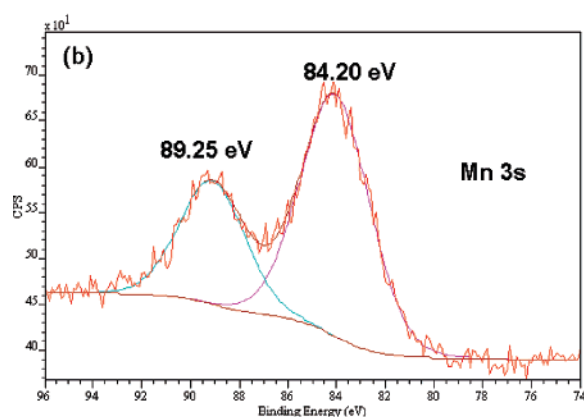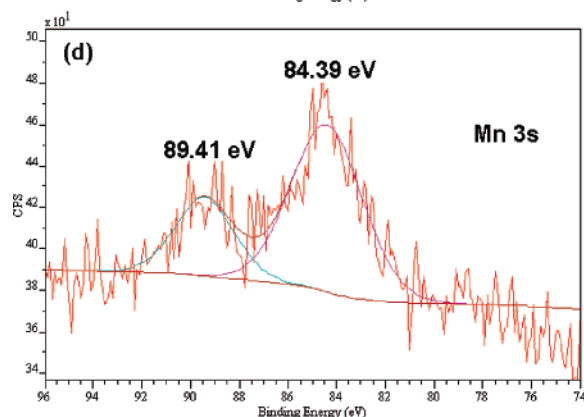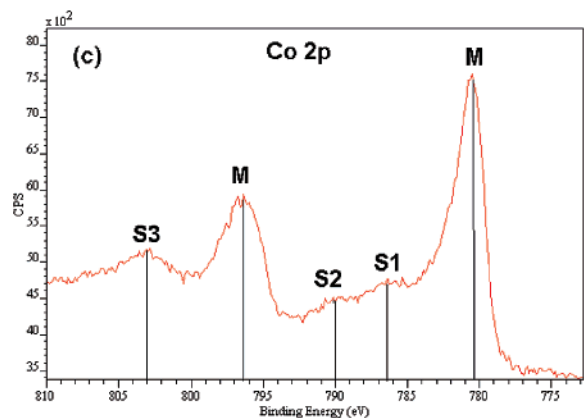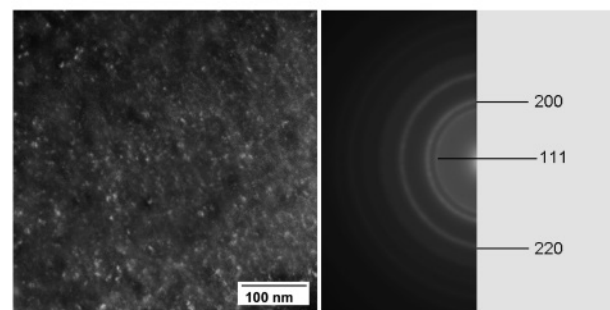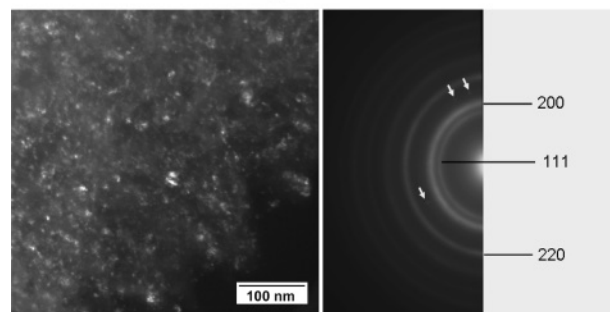
### (b) Pure Mn (II)

### (c) and (d) Co:Mn = 29:1

**Figure 2.** XPS spectra for manganese−cobalt oxides prepared from various solutions: (a) pure Co(II); (b) pure Mn(II); (c, d) Co:Mn = 29:1.
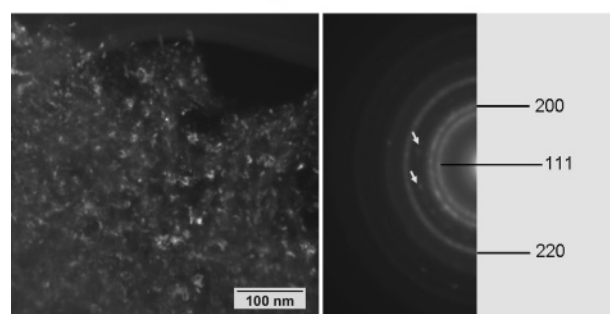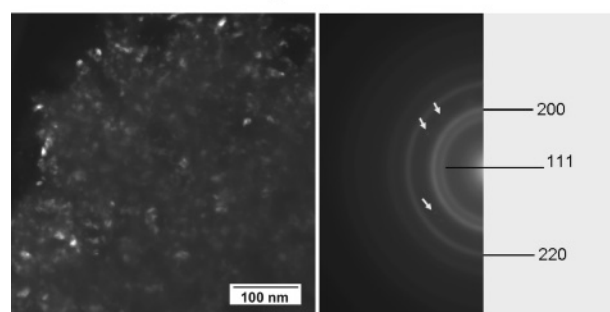


**Figure 3.** Representative DFTEM images and diffraction patterns for oxides prepared from various solutions: (a) pure cobalt oxide; (b) Co: Mn = 29:1; (c) Co:Mn = 1:1; (d) Co:Mn = 1:9; (e) pure manganese oxide.

Rock-Salt Structure in Mn−Co−O Nanocrystals

*J. Phys. Chem. C, Vol. 111, No. 28, 2007* **10401**

**TABLE 2: Co 2p Binding Energies (eV) for Oxides Prepared from Co(II)-Containing Solutions**[a]

| | Co $2p_{3/2}$ | | | | | Co $2p_{1/2}$ | | | |
|---|---|---|---|---|---|---|---|---|---|
| sample | $M$ | $S1$ | $S2$ | $\Delta S1$ | $\Delta S2$ | $M$ | $S3$ | $\Delta S3$ | spin−orbit splitting (eV) |
| pure Co(II) | 780.3 | 786.2 | 790.1 | 5.9 | 9.8 | 795.3 | 804.9 | 9.6 | 15.0 |
| Co:Mn = 29:1 | 780.4 | 786.4 | 789.9 | 6.0 | 9.5 | 796.0 | 803.0 | 7.0 | 15.6 |

[a] $M$ = binding energy of the main peak, $S$ = binding energy of the satellite peaks, and $\Delta S$ = energy separation between the main peak and satellite peaks.
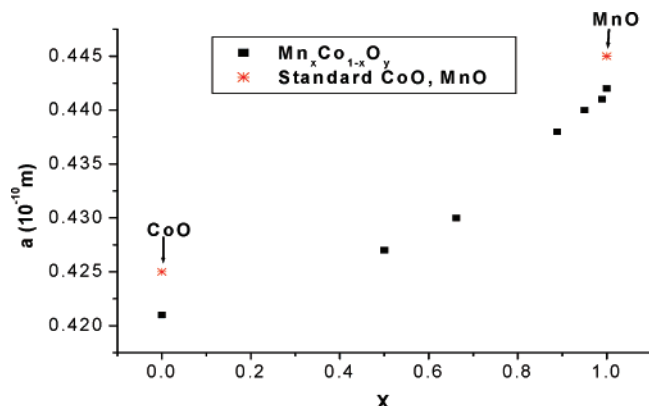


**Figure 4.** Lattice parameters for as-deposited oxides plotted as a function of the deposit Mn:Co ratio.



**Figure 5.** Intensity profiles for experimental SAD ring patterns of as-deposited oxides.

Core-level Mn 3s spectra of pure manganese oxides and mixed manganese−cobalt oxides (Co:Mn = 29:1) are shown in Figure 2b,d. The doublet Mn 3s peaks are the result of parallel spin coupling between electrons in the 3s and 3d orbitals. The oxidation states of Mn are closely related to the 3s peak splitting widths. When the valence of the Mn cations decreases, i.e., more electrons exist in the 3d orbitals, the splitting width increases.[28,29] The experimental splitting widths ($\Delta E$) in Mn 3s spectra of pure manganese oxides and mixed manganese−cobalt oxides (Co: Mn = 29:1) are 5.05 and 5.02 eV, which correspond to an average oxidation valence of 3.5 on the basis of an approximately linear relationship between the splitting width ($\Delta E$) and the Mn oxidation state.[28−32] From the WDS results and the XPS analysis, $Mn_2O_3/MnO_2$ phases are expected to exist in pure electrodeposited manganese oxides and mixed manganese−cobalt oxides (Co:Mn = 29:1).

**Structural Characterization.** A series of representative dark-field transmission electron microscopy (DFTEM) images and diffraction patterns from the as-deposited oxides, ranging from pure cobalt oxides to manganese oxides, are shown in Figure 3. The DF micrographs show that the oxides are composed of nanocrystalline oxide particles with diameters of less than 10 nm. The corresponding electron diffraction patterns confirm the nanocrystalline nature and a similar fcc-type structure for all the oxides, which is consistent with previous work.[13] The lattice parameters of the oxides were estimated, on the basis of an fcc unit cell, and plotted against the Mn:Co ratio (Figure 4). The symmetry of the diffraction patterns suggests that an oxide structure could be described as a face-centered cubic array of oxygen anions with Mn−Co cations occupying the tetrahedral and octahedral interstices. If the cations occupy all eight tetrahedral interstices in the unit cell, then an antifluorite-type structure is formed. The oxygen anion to metal cation ratio is 1:2 in the antifluorite-type unit cell. When all four octahedral sites are occupied, a rock-salt-type (NaCl) structure is expected. The oxygen anion to metal cation ratio is 1:1 in the rock-salt-type unit cell. When cations occupy both the tetrahedral and octahedral sites, the structure can be a mixture of the antifluorite and rock-salt structures. On the basis of
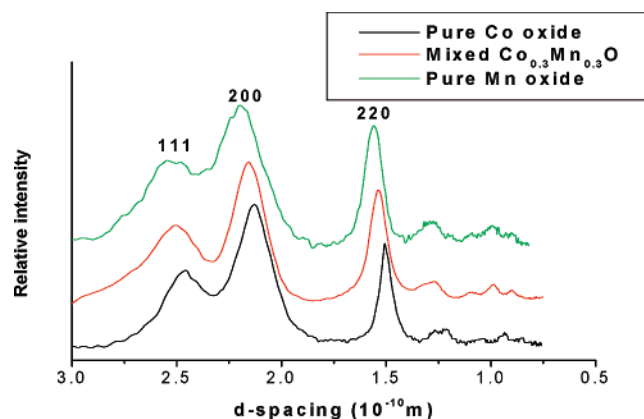
the WDS and XPS analysis, the anion to cation ratio is in the 1.47−1.79 range, which is significantly higher than what would be expected for purely antifluorite or rock-salt structures. This result suggests that the interstitial positions are not fully occupied.

To unambiguously understand the crystal structure of the oxide nanocrystals, the intensity of the observed SAD ring patterns needs to be taken into account. Simulated SAD ring patterns were calculated for three model structures on the basis of a kinematical approximation[14] using Desktop Microscopist software. It was assumed that the Co−Mn cations occupy the octahedral and/or tetrahedral lattice interstices randomly. The diffracted intensity profiles of the observed and simulated SAD ring patterns were obtained using ImageJ 1.37 software. Figure 5 compares the intensity profile of some experimental SAD ring patterns. Very similar intensity profiles were obtained as the oxide composition was varied from pure cobalt oxide to pure manganese oxide. The oxide Co:Mn ratios do not influence the profile shape, only the diffraction peak position. Because the reflections lose intensity rapidly with increasing scattering angle due to multiple scattering effects,[14] only the first three strongest reflections are discussed further. The most remarkable feature in Figure 5 is the characteristic weak intensity of the (111) reflection, compared with the strongest (200) and second strongest (220) reflections.

Since the ratio of metal cations to oxygen anions in the oxides is less than unity, i.e., the oxides are cation deficient, cations as well as vacancies must be included when electron scattering from the interstitial sites is considered. A similar treatment has been applied to determine spinel-to-rock-salt structural phase transformation in $MgAl_2O_4$ induced by ion irradiation.[33] In the antifluorite-type unit cell (tetrahedral occupancies), the cation deficiency would be 65−72% on the basis of the WDS results (Table 1) if all tetrahedral sites are considered. Figure 6 depicts the intensity profiles for simulated SAD ring patterns based on an antifluorite-type structure for pure cobalt oxide, pure manganese oxide, and a mixed manganese−cobalt oxide. The same profile shape is apparent for all three oxides. It is clear
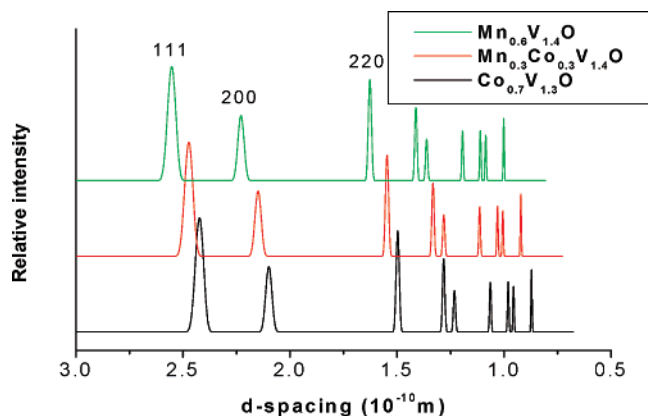
**Figure 6.** Intensity profiles for simulated SAD ring patterns for CoO, MnO, and mixed manganese−cobalt oxides (tetrahedral occupancies). The symbol "V" represents vacancies in interstitial positions.
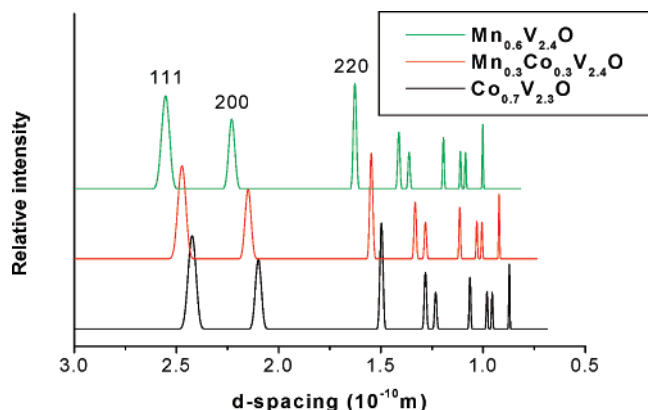


**Figure 7.** Intensity profiles for simulated SAD ring patterns for CoO, MnO, and mixed manganese−cobalt oxides (both tetrahedral and octahedral occupancies). The symbol "V" represents vacancies in interstitial positions.



**Figure 8.** Intensity profile for simulated SAD ring patterns based on the rock-salt-type structure for CoO, MnO, and mixed manganese−cobalt oxides (octahedral occupancies). The symbol "V" represents vacancies in interstitial positions.

that the (220) reflection is slightly weaker than the strongest reflection (111), but much higher than the (200) reflection. This feature is not consistent with the observed SAD ring patterns (Figure 5).

When the Co−Mn cations occupy both the octahedral and tetrahedral lattice interstices randomly, the estimated cation deficiency (or percentage of vacancies) is 77−82%. Figure 7 shows intensity profiles for simulated SAD ring patterns for pure cobalt oxide, pure manganese oxide, and mixed manganese−cobalt oxide with the appropriate number of cation vacancies. The predicted (200) and (220) reflection intensities increase when octahedral sites are occupied by metal cations, whereas the (111) reflection intensity is suppressed. The peak intensities decrease in the following order: (220) > (111) > (200). This is still not consistent with the observed SAD ring patterns (Figure 5).

Simulated SAD ring patterns, based on the rock-salt-type unit cell with only octahedral occupancies, were obtained. On the basis of the WDS results in Table 1, the cation deficiency (percentage of vacancies) is in the 30−45% range. Figure 8 shows the intensity profiles for simulated SAD ring patterns with a rock-salt-type structure with the appropriate number of vacancies. Compared with Figure 7, the (111) reflection is further suppressed, and the (200) reflection has surpassed the (220) reflection to become the strongest one (Figure 8). The experimental SAD patterns from the as-deposited oxides (Figure 5) are in good agreement with the simulated SAD patterns for a defective rock-salt-type structure containing cation vacancies (Figure 8). Therefore, it is reasonable to conclude that the as-
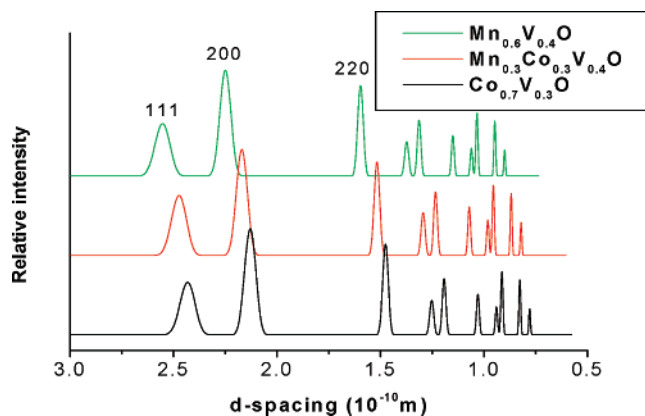
deposited oxides, from pure cobalt oxide to pure manganese oxide, have a defective rock-salt-type structure with Mn and Co ions, as well as vacancies, occupying octahedral sites.

From Figure 4, it is apparent that the lattice parameters for the as-deposited cobalt oxide (0.421 nm) and manganese oxide (0.442 nm) are smaller than those for standard CoO (0.425 nm) and MnO (0.445 nm). This difference in unit cell size can be attributed to the shorter cation−anion bond length for as-deposited oxides with a significant number of cation vacancies. In addition to the normal rock-salt diffraction rings, there are some extra diffracted spots between the (200) and (220) reflections in the Mn-rich oxides, as shown with white arrows in Figure 3c−e. The *d* spacings for the extra diffracted spots are not consistent with any reflections for existing stable manganese oxide phases. Furthermore, the *d* spacings of the extra diffracted spots change with the lattice parameters of the rock-salt-type unit cell, so they appear to correlate with the forbidden (211) reflection. Note that the extra diffracted spots disappear as the Co content further increases in the oxide nanocrystals. The extra diffracted spots may be attributed to partial ordering of Mn vacancies. Simulated SAD patterns based on the defective rock-salt-type unit cell with Mn vacancy ordering were also calculated. Various percentages of vacancies, ranging from 0% to 100%, were assumed to be ordered on two specific octahedral positions and with the remaining vacancies occupying the other two octahedral positions randomly. In addition to the allowed reflections for the rock-salt-type unit cell, other reflections including the (211) reflection appear in the simulated SAD patterns (not shown here). Ordering of some of the Mn vacancies would alter the rock-salt-type symmetry. The formation of this type of defective rock-salt-type structure is likely a consequence of the low-temperature process for electrodepositing the oxides. The thermal energy is not sufficient to overcome the energy barrier to form equilibrium phases such as $Co_3O_4/Co_2O_3$, $Mn_2O_3/MnO_2$, or spinel-type manganese−cobalt oxides.

## Conclusions

Detailed structural characterization of anodically deposited Mn−Co−O nanocrystals, ranging in composition from pure cobalt oxide to pure manganese oxide, was conducted using WDS, XPS, and TEM. WDS and XPS analyses suggest that there is an inherent cation deficiency associated with all the as-deposited oxides. SAD ring patterns obtained from these oxides indicate that the (111) reflection is much weaker than

Rock-Salt Structure in Mn−Co−O Nanocrystals

*J. Phys. Chem. C, Vol. 111, No. 28, 2007* **10403**

the (200) and (220) reflections. This observation is consistent with simulated SAD ring patterns of a defective rock-salt-type phase, in which cation vacancies reside on some of the octahedral interstices. Extra diffracted spots were also observed between the (200) and (220) reflections, which can be attributed to the ordered distribution of Mn vacancies in the rock-salt-type unit cells. The formation of this type of defective rock-salt structure is likely related to the low processing temperatures for oxide formation.

**References and Notes**

(1) Buhl, R. *J. Phys. Chem. Solids* **1969**, *30*, 805−812.
(2) Boucher, B.; Buhl, R.; di Bella, R.; Perrin, M. *J. Phys.* **1970**, *31*, 113.
(3) Naka, S.; Inagaki, M.; Tanaka, T. *J. Mater. Sci.* **1972**, *7*, 441−444.
(4) Jimenez-Mateo, J. M.; Morales, J.; Tirado, J. L. *J. Solid State Chem.* **1989**, *82*, 87−94.
(5) Martin de Vidales, J. L.; Garcia-Martinez, O.; Vila, E.; Rojas, R. M.; Torralvo, M. J. *MRS Bull.* **1993**, *28*, 1135−1143.
(6) Rojas, R. M.; Vila, E.; Garcia-Martinez, O.; Martin de Vidales, J. L. *J. Mater. Chem.* **1994**, *4*, 1635−1639.
(7) Martin de Vidales, J. L.; Vila, E.; Rojas, R. M.; Garcia-Martinez, O. *Chem. Mater.* **1995**, *7*, 1716−1721.
(8) Vila, E.; Rojas, R. M.; Martin de Vidales, J. L.; Garcia-Martinez, O. *Chem. Mater.* **1996**, *8*, 1078−1083.
(9) Zhang, H. T.; Chen, X. H. *Nanotechnology* **2006**, *17*, 1384−1390.
(10) Zhang, Z. J.; Wang, Z. L.; Chakoumakos, B. C.; Yin, J. S. *J. Am. Chem. Soc.* **1998**, *120*, 1800−1804.
(11) Chen, J. P.; Sorensen, C. M.; Klabunde, K. J.; Hadjipanayis, G. C.; Devlin, E.; Kostikas, A. *Phys. Rev. B* **1996**, *54*, 9288−9296.
(12) Chuang, P. Y.; Hu, C. C. *Mater. Chem. Phys.* **2005**, *92*, 138−145.
(13) Wei, W.; Chen, W.; Ivey, D. G. *Chem. Mater.* **2007**, *19*, 2816−2822.

(14) Hirsch, P.; Howie, A.; Nicholson, R. B.; Pashley, D. W.; Whelan, M. J. *Electron Microscopy of Thin Crystals*; Robert E. Krieger Publishing Co., Inc.: New York, 1977.
(15) Kim, K. S. *Phys. Rev. B* **1975**, *11*, 2177−2185.
(16) Barreca, D.; Massignan, C.; Daolio, S.; Fabrizio, M.; Piccirillo, C.; Armealo, L.; Tondello, E. *Chem. Mater.* **2001**, *13*, 588−593.
(17) Gulino, A.; Fiorito, G.; Fragala, I. *J. Mater. Chem.* **2003**, *13*, 861−865.
(18) Gulino, A.; Dapporto, P.; Rossi, P.; Fragala, I. *Chem. Mater.* **2003**, *15*, 3748−3752.
(19) Pasko, S.; Abrutis, A.; Hubert-Pfalzgraf, L. G.; Kubilius, V. *J. Cryst. Growth* **2004**, *262*, 653−657.
(20) Pasko, S.; Hubert-Pfalzgraf, L. G.; Abrutis, A.; Vaissermann, J. *Polyhedron* **2004**, *23*, 735−741.
(21) Cataldi, T. R. I.; Gasella, I. G.; Desimoni, E.; Rotunno, T. *Anal. Chim. Acta* **1992**, *270*, 161−171.
(22) Valeri, S.; Borghi, A.; Gazzadi, G. C.; di Bona, A. *Surf. Sci.* **1999**, *423*, 346−356.
(23) Shen, Z. X.; Allen, J. W.; Lindberg, P. A. P.; Dessau, D. S.; Wells, B. O.; Borg, A.; Ellis, W.; Kang, J. S.; Oh, S. J. *Phys. Rev. B* **1990**, *42*, 1817−1828.
(24) Jimenez, V. M.; Fernendz, A.; Espinos, J. P.; Gonzalez-Elipe, A. R. *J. Electron Spectros. Relat. Phenom.* **1995**, *71*, 61−71.W
(25) Ernst, B.; Libs, S.; Chaumette, P.; Kiennemann, A. *Appl. Catal., A* **1999**, *186*, 145−168.
(26) Gastner, D. G.; Watson, P. R.; Chan, I. Y. *J. Phys. Chem.* **1989**, *93*, 3188−3194.
(27) Burriel, M.; Garcia, G.; Santiso, J.; Abrutis, A.; Saltyte, Z.; Figueras, A. *Chem. Vap. Deposition* **2005**, *11*, 106−111.
(28) Carver, J. C.; Schweitzer, G. K.; Carlson, T. A. *J. Chem. Phys.* **1972**, *57*, 973−982.
(29) Chigane, M.; Ishikawa, M. *J. Electrochem. Soc.* **2000**, *147*, 2246−2251.
(30) Toupin, M.; Brousse, T.; Be'langer, D. *Chem. Mater.* **2002**, *14*, 3946−3952.
(31) Djurfors, B.; Broughton, J. N.; Brett, M. J.; Ivey, D. G. *Acta Mater.* **2005**, *53*, 957−965.
(32) Nakayama, M.; Tanaka, A.; Sato, Y.; Tonosaki, T.; Ogura, K. *Langmuir* **2005**, *21*, 5907−5913.
(33) Ishimaru, M.; Afanasyev-Charkin, I. V.; Sickafus, K. E. *Appl. Phys. Lett.* **2000**, *76*, 2556−2558.